





Cite this: *Ind. Chem. Mater.*, 2024, 2, 458

An electron beam irradiation-assisted coating method for the regulation of hydrophilicity and hydrophobicity†

Haozhe Li, ^a Keyan Sheng, ^{ac} Zhiyan Chen,^b Shuai Hao,^b Zijian Zhou,^a Zhenyi Zhang,^a Xinwen Liu,^a Mianzhi Xiong,^a Yanlong Gu ^{*b} and Jiang Huang ^{*a}

Developing a stable, reliable, and industrially compatible method to control hydrophobicity is crucial for separation, transportation, and the generation of special surfaces. An e-HMS-PDMS silica gel nanoparticle coating was prepared using a two-step electron beam irradiation (EBI) process, consisting of (i) grafting of two organic groups onto thiol-functionalized hollow mesoporous silica (HMS-SH) with 10 MeV EBI and (ii) curing of polydimethylsiloxane (PDMS) onto silicone rubber using the HMS hybrid materials prepared in step i as an additive with 200 keV EBI. The tuneable grafting of functional groups and the surface properties of the silica, which was embedded in the PDMS layer, allowed us to precisely control the hydrophilicity of the PDMS layer by means of altering the grafting gradient of the silica and the loading ratio of the monomers. A diverse range of vinyl-structured monomers can be used in this method, and the selection of suitable monomers is vital in determining the physical properties of the coating layer. The hydrophilicity of the coating can be linearly controlled within a specific range (50° to 155°) by using suitable monomers, allowing for the design of surfaces with specific hydrophilic and hydrophobic requirements.

Keywords: Electron beam irradiation; Nanoparticle composite coating; Hydrophilicity/hydrophobicity; Thiol-ene click reaction.

Received 1st February 2024,
Accepted 25th April 2024

DOI: 10.1039/d4im00015c

rsc.li/icm

1 Introduction

Both hydrophilic and hydrophobic surfaces play a crucial role in engineering applications. Hydrophilic surfaces facilitate rapid liquid spreading,¹ while hydrophobic surfaces promote the formation of microdroplets or bead-like structures. The regulation of material surface hydrophilicity facilitates the development of anti-pollution coatings,^{2,3} control over biomaterial–cell interactions,⁴ and various wetting and separation technologies.^{5,6} Surface hydrophilicity also impacts liquid transport and heat conduction,⁷ enhancing the performance of heat exchange equipment and batteries.^{8,9} Additionally, it influences the design and application of heterogeneous catalysts¹⁰ and functional nanoparticles (NPs).¹¹ Hence, accurate regulation of surface hydrophilicity

holds significant potential for diverse applications across various fields.

A variety of external stimulation methods can regulate the hydrophobicity of surfaces,¹² including the application of electrostatic fields^{13,14} and electrochemical switches,¹⁵ or the utilization of specific wavelengths of light to alter the contact angle of material surfaces.^{16,17} Additionally, thermal¹⁸ and mechanical switching¹⁹ represent potential methodologies. The challenges of the above methods arise from the instability of these external stimuli, the manufacturing cost of the corresponding device, and the limited range of surface contact angle control. Similarly, chemical modification^{20–22} and plasma spraying techniques²³ are employed to augment the hydrophilicity of surfaces to achieve desired surface properties. The above methods often encounter difficulties in achieving the specific contact angle requirements for a stable interface. A simple and reliable method is therefore still needed to accurately control coating hydrophilicity.

Electron beam irradiation (EBI) technology is a scalable physical method widely used in the food²⁴ and chemical industries,²⁵ offering advantages such as the absence of chemical initiators,²⁶ high efficiency, and environmental friendliness.²⁷ An appropriate energy electron beam can initiate the desired radical reactions, leading to molecular cross-

^a State Key Laboratory of Advanced Electromagnetic Technology, Huazhong University of Science and Technology, Wuhan 430074, Hubei, PR China.

E-mail: jhuang@hust.edu.cn

^b Hubei Key Laboratory of Material Chemistry and Service Failure, School of Chemistry and Chemical Engineering, Huazhong University of Science and Technology, Wuhan 430074, Hubei, PR China. E-mail: klgyl@hust.edu.cn

^c Huadian Electric Power Research Institute Co., Ltd, Hangzhou 310030, China

† Electronic supplementary information (ESI) available. See DOI: <https://doi.org/10.1039/d4im00015c>



linking, grafting,^{28,29} and alteration of the material properties.³⁰ The pioneering thiol-ene reaction, triggered by electron beams, modifies fibers and films,^{31,32} enabling surface property alterations across various materials. Simultaneously, the *in situ* curing of PDMS by electron beams is primer-free and rapid, and exhibits loadable characteristics.³³

In this study, thiol-ene click grafting between hollow mesoporous silica (HMS) and two monomers with different polarities was initiated using a 10 MeV accelerator. By adjusting the volume ratio of the monomer solutions, graded grafting rates can be achieved for the hybrid materials. With the incorporation of HMS microspheres as a core additive, the e-HMS-PDMS coatings underwent rapid curing within seconds under 200 keV EBI. By changing the vinyl-containing monomers and their loading ratio, the hydrophilicity of the generated e-HMS-PDMS coating can be tuned to some extent. The EBI technology enables grafting and curing in just seconds, without the need for chemical initiators or heating processes. This, combined with the coating's stability, gives it potential for industrial use.

2 Results and discussion

2.1 Characterization of the EBI-grafted hybrid material G1 series

In the coating method outlined in this study (Fig. 1), the grafted HMS hybrid materials G1–G5 exhibit varying grafting rates on their respective selected monomers, thereby influencing the physicochemical properties of the additives and subsequently impacting the hydrophilicity of the e-HMS-PDMS coatings. All of the additives, G1–G5, were fully characterized by physicochemical methods to make sure that the EBI grafting of HMS was successful. For simplicity, in this part, G1 was selected as an illustrative example to show the

details of material analysis. The G1 additives G1 were synthesized by using a mixture composed of 3-sulfolene and octadec-1-ene as the grafting reagent. From G1–0 to G1–6, the volume ratios of 3-sulfolene to octadec-1-ene was changed from 10:0 to 9:1, 7:3, 5:5, 3:7, 1:9, and 0:10, respectively.

The FTIR spectra of the hybrid materials in the G1 series are shown in Fig. 2a. A weak peak appears at 1309 cm^{-1} from G1–0 to G1–5, which can be assigned to the antisymmetric stretching vibration absorption peak of $\text{O}=\text{S}=\text{O}$,³⁵ while the possible stretching vibration absorption peak of $\text{O}=\text{S}=\text{O}$ that appears near 1160 cm^{-1} is covered by the strong stretching vibration absorption peak of silicone $\text{Si}-\text{O}-\text{Si}$. The intensity of the saturated CH_2 antisymmetric and stacked stretching absorption peaks³⁶ at 2925 cm^{-1} and 2855 cm^{-1} increased from G1–1 to G1–6 with the increase in volume proportion of 1-octadecene, while the weak S–H peak of mercaptan at 2563 cm^{-1} disappeared for HMS-SH.³⁷ The FTIR spectra in Fig. 2a indicate that the EBI-based grafting of monomers onto the HMS materials is indeed successful, and by changing the original loading ratio of the two monomers, a clear difference in terms of the density of grafted groups can be found.

The TGA curves of the hybrid materials of the G1 series are presented in Fig. 2b. All of the materials exhibit a quite similar trend of thermogravimetric loss. The abrupt thermogravimetric loss is concentrated between $300\text{ }^\circ\text{C}$ and $400\text{ }^\circ\text{C}$, where the grafted organic matter is rapidly lost. The residual weight of the G1 material decreases from 70.5% to 59.9%. This can be ascribed to the high molecular weight of octadec-1-ene (252.48) compared to 3-sulfolene (118.15). In G1–1 to G1–5, as the amount of grafted octadec-1-ene increases, the heat loss of the organic matter becomes more significant. The results obtained from thermogravimetry

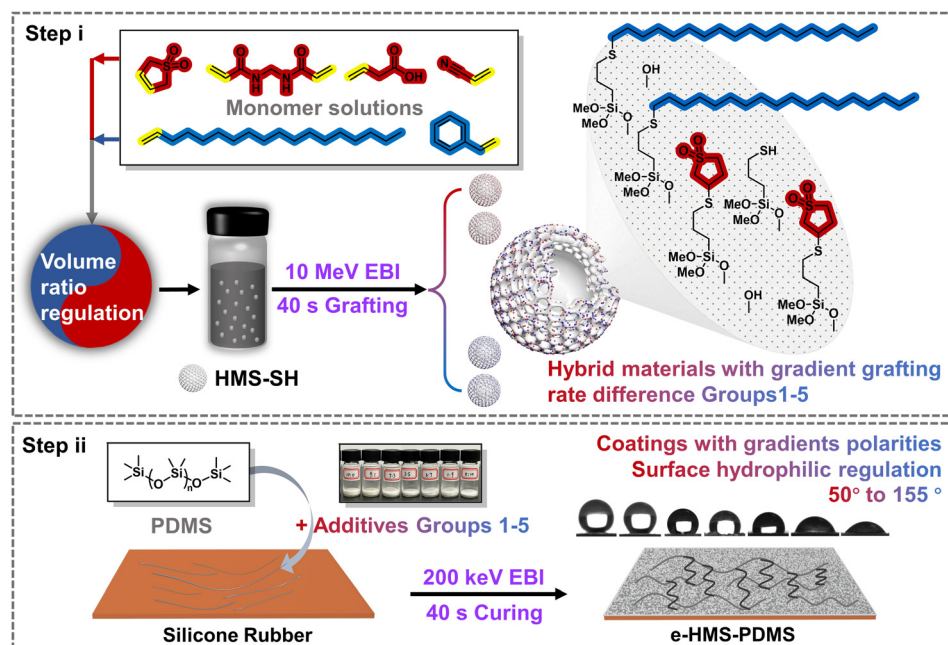


Fig. 1 Schematic illustration of the coating method for the preparation of e-HMS-PDMS by electron beam irradiation.



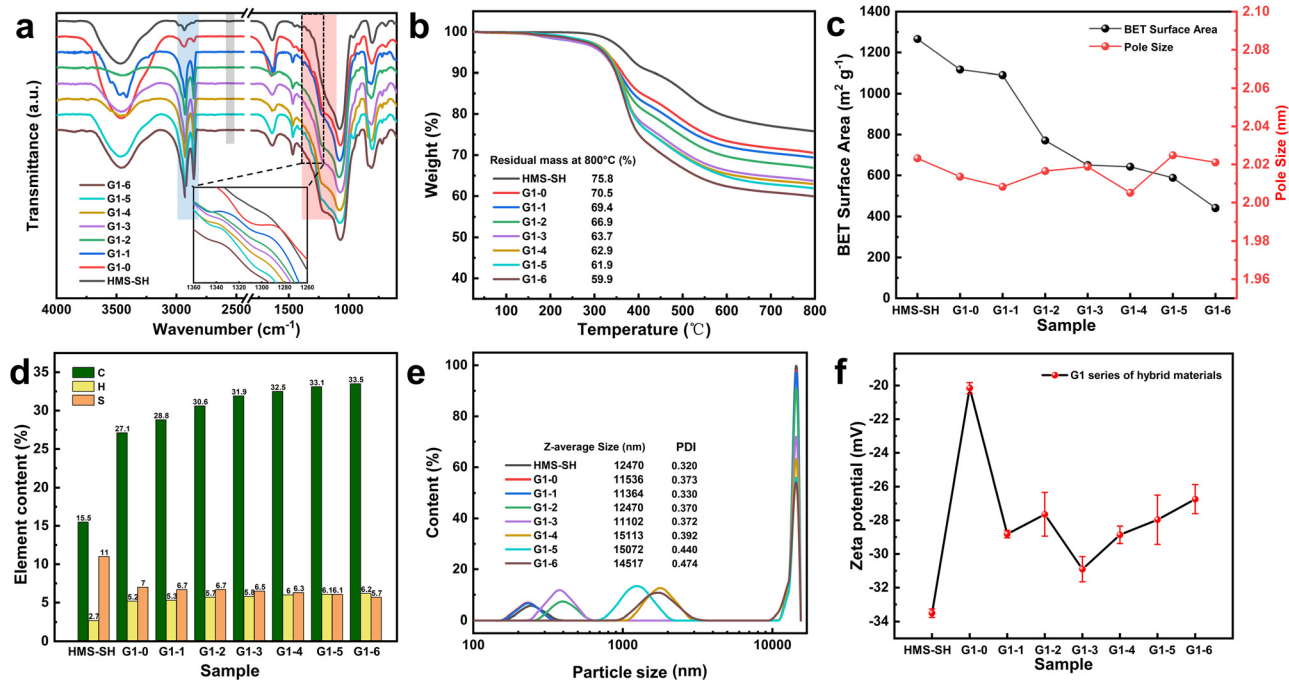


Fig. 2 The physical and chemical properties of the hybrid materials of the G1 series. (a) FTIR spectra; (b) TGA curves; (c) BET adsorption specific surface area and pore size; (d) elemental analysis; (e) particle size distribution curves; (f) zeta potential measurements.

analysis allowed us to estimate the grafting densities of 3-sulfolene and octadec-1-ene of the hybrid material. For G1-0, the grafted 3-sulfolene was estimated to be 0.45 mmol g^{-1} , and for G1-6, the grafted octadec-1-ene is 0.63 mmol g^{-1} . The results indicated also that the grafting rate of the two monomers can indeed be regulated in this EBI-based surface modification method.

The specific surface areas of the hybrid materials of the G1 series and their calculated pore sizes are depicted in Fig. 2c. The average pore size of the hybrid materials remains virtually unaltered, but their specific surface area exhibits a downward trend with the increase in the volume ratio of octadec-1-ene. Nonetheless, the minimal value of their specific surface area is still higher than $440 \text{ m}^2 \text{ g}^{-1}$.

Fig. 2d directly exhibits the elemental composition of carbon, hydrogen, and sulfur in the hybrid materials of the G1 series. Compared to HMS-SH, the content of the carbon and hydrogen elements in the grafted materials is augmented, whereas the sulfur element content diminished. As the monomer volume ratio varied, the carbon element content in the G1 series escalated progressively, whereas the elemental sulfur content demonstrated a downward tendency. The specific values of the content for each element are presented in Table S1.†

The particle size distribution curve is presented in Fig. 2e. The average particle size of the hybrid materials of the G1 series ranges from tens to thousands of nanometers, exhibiting a combination of large and small microspheres. As the proportion of modifier varies, the population of smaller-sized microspheres increases, leading to an overall increase in the average particle size and alterations in the uniformity

of the particle size distribution. A higher volume ratio of 1-octadecene corresponds to more fragmented silicon microspheres and a greater degree of unevenness in the particle size distribution.

Based on zeta potential analysis (Fig. 2f), HMS-SH exhibits an overall negative charge because of the presence of unpaired electrons on its surface, modified with mercaptan groups. While there is a slight increase in zeta potential during the irradiation grafting process, the changes in the volume ratio of the grafted monomer do not exhibit consistent patterns within a certain range, possibly due to the absence of inherent charge on the monomer itself. The particle size distribution and zeta potential data for G2–G5 are presented in Table S3.† The results above demonstrate the successful induction of a mercaptan click grafting reaction between the silicon microspheres and the two monomers using electron beam. Additionally, the grafting rate can be controlled by adjusting the volume ratio of the monomers.

The XRD pattern of the G1 series additives in Fig. 3 exhibits a prominent peak at 2.36° and a broad, flat peak at around 22.30° . The peak characterized by a small angularity in Fig. 3b signifies the pore structure information present in the HMS material.^{38,39} In comparison to HMS-SH, the intensity of the grafted NP peak is notably diminished, and its apex shifts towards a smaller angularity. This alteration in the peak's characteristics suggests modifications to the pore structure,^{40,41} which may lead to a change in the specific surface area of BET adsorption. Fig. 3c displays an amorphous peak at approximately 22.30° . As the volume of octadec-1-ene monomer increases, the peak strength progressively escalates, suggesting that the quantity



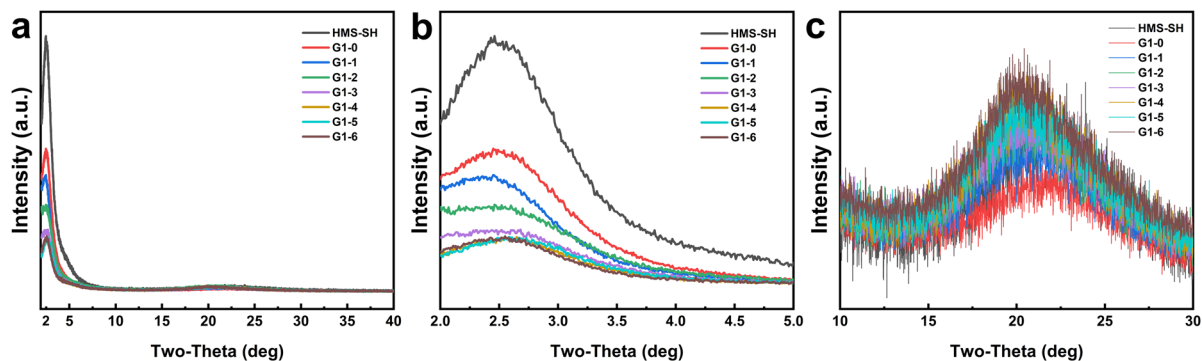


Fig. 3 The XRD patterns of the hybrid materials of the G1 series. (a) 2–40 degrees; (b) 2–5 degrees; (c) 10–30 degrees.

of amorphous organic matter in the materials correspondingly augments.⁴² Overall, the EBI-based grafting of organic moieties does not alter the structural framework of the HMS-based materials. However, the grafting density of each organic monomer on the hybrid material can be manipulated to some extent by changing the volume ratio of the vinyl-containing monomer. The other hybrid materials obtained were also analyzed using XRD, and the corresponding results are shown in Fig. S12.† The influence of different monomers on the properties of these hybrid materials follows a similar trend as observed in the G1 series.

To shed light on the grafting reaction mechanism, electron paramagnetic resonance (EPR) testing was employed to identify the specific types of free radicals generated by EBI. A free radical scavenger, 5,5-dimethyl-1-pyrroline *N*-oxide (DMPO), was quantitatively added to the solution containing grafted monomers. DMPO possesses a ·NO oxidation center and contains several conjugated π -electron systems in its molecular structure, thereby exhibiting a strong affinity for other free radicals and forming stable free radical admixtures with them. Consequently, the application of an EPR magnetic field reveals distinct characteristics of unpaired electrons. Upon incidence of the electron beam on the system, a large number of electrons activate the grafting reagent in the solution system, generating free radicals that form adducts with DMPO (Fig. 4).

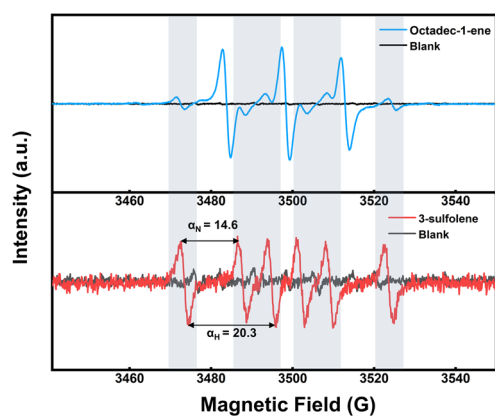


Fig. 4 The EPR spectra of octadec-1-ene and 3-sulfolene solutions during EBI.

In comparison to the pure solvent without grafting reagent, typical vinyl free radical signals are observed, along with coupling constants $\alpha_N = 14.6$ G and $\alpha_H = 20.3$ G, indicating the generation of vinyl free radicals by the monomer during irradiation.^{43–45} In a vinyl monomer solution, high-energy electrons effectively excite numerous vinyl radicals within a remarkably short time, promoting their reaction with modified sulfhydryl groups on the HMS microspheres and ultimately leading to covalent bond grafting.

The FSEM images of the G1 series hybrid materials are shown in Fig. 5, including the HMS-SH before grafting and G1-1, G1-3, and G1-5 with monomer ratios of 9 : 1, 5 : 5, and 1 : 9, respectively. Fig. 5a and b showcase the HMS-SH materials,⁴⁶ which are spherical materials with a diameter of about tens of microns. Some of these materials exhibit hemispherical shapes and irregularities. In contrast, G1-1 exhibits no significant variation in Fig. 5c, while G1-3, depicted in Fig. 5d, maintains a similar spherical morphology until the volume ratio of octadec-1-ene reaches 90% *i.e.*, G1-5. As shown in Fig. 5e and f, some fragments are adhered to the spherical particles. The FSEM images revealed that the microstructure of the HMS series hybrid materials remained unaffected by irradiation grafting-induced functional group formation. With a change in monomer, particle aggregation may occur due to fragment-induced interactions. In Fig. S13,† the TEM images of the small microspheres with a diameter of hundreds of nanometers reveal the nature of the complex pore structure and hollow shell structure of this series of silicon microspheres.

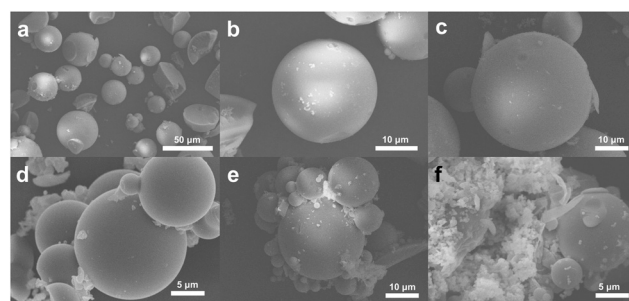


Fig. 5 The FSEM images of the hybrid materials of the G1 series. (a and b) HMS-SH; (c) G1-1; (d) G1-3; (e and f) G1-5.



The distribution of elements on the surface of the hybrid material in Fig. 6 was further analysed using the EDS mapping spectrum based on the FSEM images provided. To quantify the surface element content to some extent, a higher magnification was used to ensure that the entire field of view is filled by the silicon microspheres. The silicon element is uniformly distributed on the material's surface, indicating a uniform grafting process. The sulfur element within the sulfhydryl group is uniformly dispersed on the surface of HMS-SH, accounting for a mass fraction of 7.37%. For comparison, the content of sulfur element on the surface of the materials varies from 7.34% in G1-1 to 5.38% in G1-3 following exposure to varying monomer volume ratios and decreases to 1.31% in G1-5. The content of carbon element also exhibits a significant increase, ranging from 31.97% in HMS-SH, 21.72% in G1-1, and 26.52% in G1-3 to 35.99% in G1-5. Further details can be found in Fig. S2–S5 and S16–S18.† In conjunction with the results of elemental analysis (Fig. 2d), the variation in volume between the two monomers during EBI grafting imparts distinct elemental content for the hybrid materials, evident both overall and on their surface.

2.2 Characterization of EBI-crosslinked PDMS

The above analysis of the hybrid materials of the G1 series demonstrates that adjusting the monomer ratio enables the preparation of mesoporous materials with varying grafting rates during EBI grafting, resulting in different properties while maintaining their structure. To exploit the microscopic gradient difference for macroscopic surface characteristic variation, the hybrid materials were incorporated as crucial additives into EBI-crosslinked PDMS to prepare a uniform e-HMS-PDMS coating.

The EBI-crosslinked PDMS serves as a robust and adhesive elastomer interface between the substrate and additives, and thereby it is crucial to optimize the formulation of PDMS and

the EBI dose. The influence of the PDMS mass fraction on its curing properties was investigated using a consistent surface dose of 600 kGy. As illustrated in Fig. 7a, the DSC curves all exhibit a single peak. Within this range, DMS functions as a *good solvent* for PDMS,⁴⁷ resulting in the formation of uniform phases in the films. Nonetheless, the endothermic peaks of 18% PDMS and 22% PDMS exhibit slightly leftward-tilted characteristics, in line with the literature's depiction of *imperfect curing*.⁴⁸ In contrast, the peaks of 26% PDMS and 30% PDMS demonstrate a rightward tilt, indicating the presence of *partial cure* attributes. The curing characteristics of the prepared samples were evaluated and are presented in Table S2,† based on DSC thermograms and dimensionless curing indexes. The TGA curves shown in Fig. 7b demonstrate thermal stability up to temperatures close to 400 °C. Coatings formulated with 24% and 26% PDMS exhibit superior temperature resistance and thermal stability at the same mass loss. The final coating formulation was determined as 24% PDMS with the best curing properties.

The radiation dose of 200 keV EBI curing not only directly affects the degree of PDMS crosslinking, but also correlates with the efficiency of e-HMS-PDMS coating preparation. The crosslinking properties of 24% PDMS were evaluated using FT-IR, DSC and TGA. In the DSC curve at 100 kGy and 0 kGy (Fig. 8a), there were distinct sharp partial peaks observed apart from the main peaks, indicating a lack of homogeneity in the PDMS and DMS phase at lower doses. As the dose gradually increased, the endothermic peak shifted towards lower temperatures, accompanied by an increase in peak width and a closer resemblance to complete curing.⁴⁹ The appropriate dose was found to be between 500 and 600 kGy. When the dose reached 1000 kGy, the endothermic peak almost disappeared. The TGA curves depicted in Fig. 8b demonstrate that the coating formulation remains consistent, indicating that the increase of the dose does not exert a significant impact on its thermal stability. A dosage of 600 kGy was determined as the irradiation curing threshold for e-HMS-PDMS. A noteworthy point is that the curing time for e-HMS-PDMS the size of an A4 sheet of paper through EBI is merely 40 s.

The FTIR spectrum in Fig. S6† reveals that the process of EBI curing did not alter the chemical bond type, while the displacement of certain peaks indicates bond reinforcement. EPR spectroscopy was employed to capture the free radicals

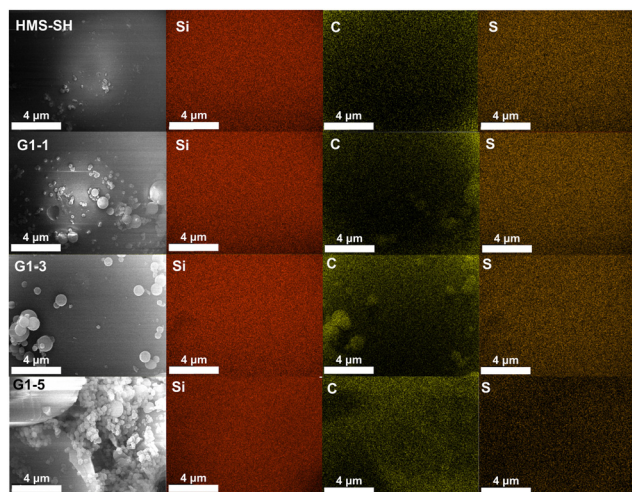


Fig. 6 The EDS mapping scan images of the hybrid materials of the G1 series.

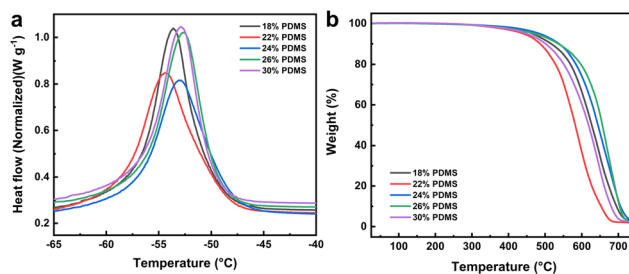


Fig. 7 The (a) DSC thermograms and (b) TGA curves of the coatings under different doses of EBI.



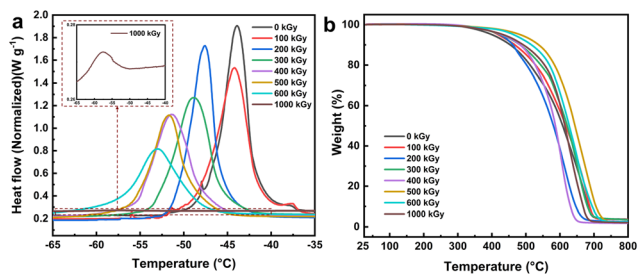


Fig. 8 The (a) DSC thermograms and (b) TGA curves of the coatings under different doses of EBI.

generated during the cross-linking of PDMS and DMS during irradiation. PDMS and trapping agent DMPO were homogenized with benzene solvent. Benzene was added before irradiation (red curve), after irradiation (blue curve), or not at all (black curve). Pure benzene served as the control (green curve). As depicted in Fig. 9, although similar experiments have been reported,^{50,51} the EPR spectrum only exhibits the phenyl radical signal upon irradiation with $\alpha_N = 14.0$ G; $\alpha_H = 21.4$ G,⁵² while other signals were negligible.

2.3 Hydrophilic and hydrophobic regulation of the e-HMS-PDMS coatings

The range of contact angle regulation, the linear fitting correlation between contact angle and monomer solution ratio, and the maximum error of contact angle measurement were used to evaluate the effect of the method described in this study on surface hydrophilicity regulation. The surface contact angles of the G1 series e-HMS-PDMS coatings (Fig. 10a) range from 50° to 155°, and the volume ratio of 3-sulfolene to octadec-1-ene monomer solution exhibits a linear correlation with an average contact angle determination coefficient $R^2 = 0.9687$. Furthermore, on the same surface, the maximum deviation in contact angle is merely 1.6 degrees. The microstructure of the irradiated cross-linked PDMS in Fig. 10b exhibits a smooth morphology, whereas the G1-3 e-HMS-PDMS coating (Fig. 10c-e) demonstrates typical nanoparticle coating characteristics, with uniformly distributed spherical additives ranging from several microns to tens of microns in diameter on the surface of the coating.

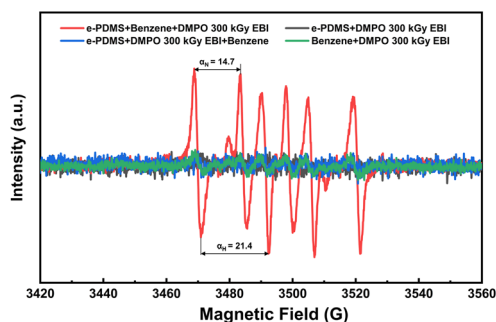


Fig. 9 The EPR spectra during EBI curing of PDMS.

Some free radical initiators such as AIBN can decompose under heating conditions, producing active free radicals and nitrogen, thereby initiating the same grafting reaction. In comparison, GC1 employs a chemical method for grafting under the same monomer concentration, aiming to contrast the merits and demerits of the two methods. The GC1 e-HMS-PDMS coating exhibits a limited hydrophilic and hydrophobic adjustment range of 74° to 142°, with a coefficient of determination $R^2 = 0.8281$ and a maximum error of 3.2 degrees on the same surface. Comparing GC1-0 (74°) with G1-0 (50°), we observed that the EBI method exhibited superior hydrophilicity, possibly due to its higher grafting rate. When the volume of octadec-1-ene exceeds 10%, irregular trends in hydrophilicity are observed in the GC1 series coatings. The hydrophilicity of GC1-2 to GC1-6 was similar, suggesting that changes in monomer concentration did not significantly affect the chemical process. Compared to chemical initiators, which have limited half-life and temperature requirements, EBI can generate numerous free radicals instantly through incident electrons without introducing any chemical pollutants into the system. The advantages of EBI in terms of efficiency and cleanness are crucial for implementing this method.

To validate the universality of the method outlined in this paper and investigate the impact of monomer selection on the coating's hydrophilicity regulation capability, 4 other series of e-HMS-PDMS coatings (G2-G5) were prepared by combining several different vinyl monomers. The only difference between the coatings of each series is the gradient difference in the volume ratio of the two monomer solutions during the hybrid material additive grafting process. Their hydrophilic and hydrophobic regulation ability are shown in Table 1.

As depicted in Fig. 11, different monomers will affect the range and precision of regulation from the perspective of grafting rate and morphology of the hybrid materials, *etc.* In addition, the differences between the two monomers must also be considered. The impact on hydrophilicity varies among polar monomers; notably, G2-0 exhibits the most hydrophilic properties. However, the G2 group exhibits the largest surface error, suggesting that certain dual vinyl structures may result in uneven grafting of the hybrid materials. This is further supported by the generally larger particle size observed in the G2 series materials (Table S3†). Although limited in scope, G3 demonstrates superior regulatory linearity and holds promise for achieving specific hydrophilicity. Conversely, when we consider different combinations involving G4 and G5 with minimal polarity differences between the monomers, this regulatory method is likely to be ineffective, thus highlighting notable discrepancies in the selection and combination of monomers for this method. Specific physical and chemical analyses pertaining to G2-G4 are presented in Fig. S8-S11.†



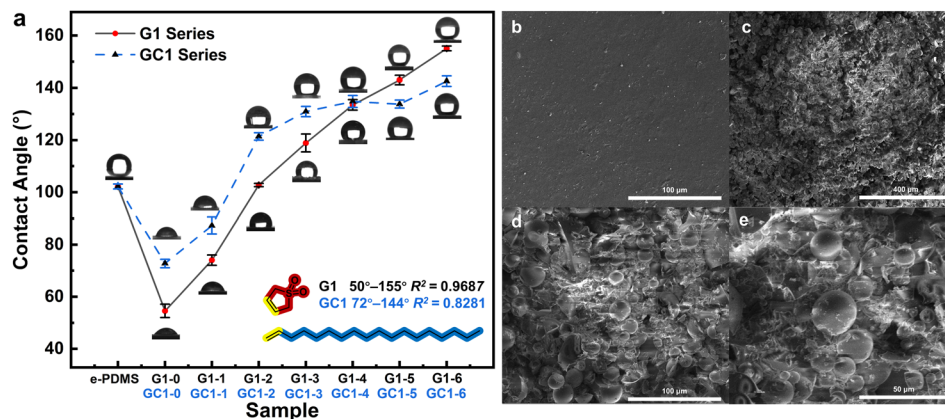


Fig. 10 The (a) contact angle test of the G1 and GC1 e-HMS-PDMS coatings; FSEM images of the (b) EBIs crosslinked PDMS and (c–e) G1–3 e-HMS-PDMS coatings.

Table 1 Hydrophobic regulation ability of different groups in this study

Entry ^a	Polar monomer	Nonpolar monomer	Regulation range	R ²	Maximum deviation
G1	3-Sulfolene	Octadec-1-ene	50–155°	0.9687	1.6°
GC1 ^b	3-Sulfolene	Octadec-1-ene	72–144°	0.8281	3.2°
G2	MBAA	Octadec-1-ene	26–155°	0.8517	16.4°
G3	Vinylacetic acid	Octadec-1-ene	78–155°	0.9908	2.9°
G4	Acrylonitrile	Styrene	86–143°	0.6815	4.5°
G5	Acrylonitrile	Octadec-1-ene	86–155°	0.8736	1.6°

^a Prepared by EBIs grafting. ^b Prepared by chemical grafting.

2.4 Stability of the e-HMS-PDMS coatings

The stability of the coating is crucial for its practical use in industry. Therefore, various properties of the coating were characterized and the results are presented in Table 2. In general, the coating exhibits superior adhesion, while the tape shows almost negligible peeling off from the X-type

grid plate with 1 mm spacing. This can be attributed to the silane-based nature of the coating, which tightly bonds with the silicone rubber surface. During impact resistance testing, despite being subjected to a fall from a height of 100 cm, both the soft texture of silicone rubber and the coating prevent any cracking or peeling off. For hardness, the coating exhibits a H-level hardness, which is considered relatively high within the realm of organic coatings. The incorporation of silicon microsphere additives significantly enhances the coating's hardness, thereby imparting better resistance to wear and scratches. The abrasion resistance test reveals that the G1 series coatings experience weight loss ranging from 4.6% to 6.8%. Fig. 12 demonstrates that initially, during the first 200 frictions, there is no significant change in contact angle and uniformity of the coating; however, afterwards they gradually decrease and deviate towards PDMS's inherent contact angle (102°), possibly due to surface damage. To enhance its abrasion resistance properties in future work, consideration can be given to adjusting the additive mass fraction.

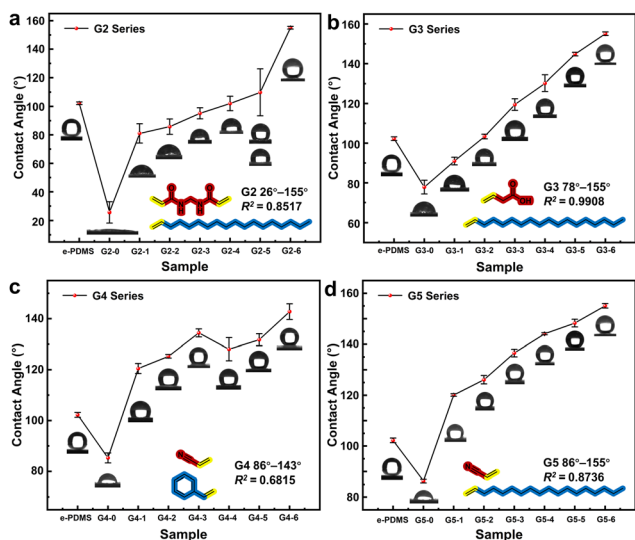


Fig. 11 The contact angle test of the (a) G2, (b) G3, (c) G4 and (d) G5 e-HMS-PDMS coatings.

Table 2 Stability test results of the e-HMS-PDMS coatings

Characterization	Executive standard	Result
Adhesion resistance test	ASTM D3359	5B
Impact resistance test	ASTM D2794	>9.81 inch-pounds
Firm hardness test	ASTM D3363	H level
Abrasion resistance test	—	Fig. 12



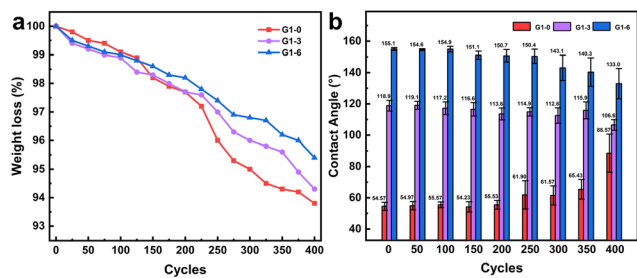


Fig. 12 The (a) abrasion cycle of the G1 series e-HMS-PDMS coatings showing the friction weight loss and (b) contact angle changes with abrasion.

Solvent stability of coating depicted in Table 3, the bonding layers of the silicone rubber substrate and silicon microsphere additive are cross-linked DMS and PDMS. The solvent resistance of the coating is limited by PDMS's chemical resistance, but it can be improved by filling the HMS silicon microspheres.⁵³ The coatings tend to swell in toluene, and exhibit improved performance in water, ethanol, dimethylformamide, and ethyl acetate.

3 Conclusion

In this study, several series of hollow mesopore silica (HMS) hybrid materials with different grafting rates of two monomers were synthesized using a thiol-ene grafting method. The grafting was realized by 10 MeV electron beam irradiation (EBI). These HMS hybrid materials are used as additives embedded in PDMS and cured using 200 keV EBI to prepare e-HMS-PDMS coatings. This two-step method allows the hydrophilicity of the silicone rubber surface to be adjusted from weakly hydrophilic to superhydrophobic. The coating exhibits excellent adhesion, and impact resistance, as well as a certain level of hardness, abrasion resistance, and solvent resistance. EBI, as a pivotal technology, enables the fabrication of coatings devoid of chemical initiators and heating processes, with completion achievable within seconds, and the HMS additives can be functionalized with various vinyl monomers. The polarity difference between the monomers leads to variations in linearity and inaccuracies in contact angle regulation. Thus, the choice of an appropriate monomer is crucial. Because of the simple operation and easy access to a wide range of monomers, it is expected that this method can be considered as an easy way to prepare tailor-made hybrid materials on the basis of specific requirements, and also to fabricate e-PDMS coatings.

Table 3 Solvent resistance test results of the e-HMS-PDMS coatings

Solvent	G1-0	G1-3	G1-6
Water	Good	Good	Good
Ethanol	Good	Good	Good
Dimethylformamide	Good	Good	Good
Ethyl acetate	Good	Good	Good
Acetone	Good	Good	Good
Toluene	Swelled	Swelled	Swelled

4 Experimental

The coating method involves two sequential steps: EBI grafting of the HMS hybrid materials and subsequent EBI curing of the nanoparticle coating to give e-HMS-PDMS. Different monomers are grafted onto the HMS-SH using an AB.10 (Wuxi El Pont, China) 10 MeV accelerator, and the final irradiation curing is completed with an EBLab 200 (Comet AG, Flamatt, Switzerland) 200 keV accelerator. The electron irradiation accelerator utilized in this study is presented in Fig. S1.† The selection of the accelerator energy was determined through a comprehensive consideration of the target reaction type and penetration depth. Monte Carlo simulation is employed to validate the electron beam's penetration depth, as depicted in Fig. S14 and S15.†

4.1 Preparation of G1–G5 series EBI-grafted hybrid materials

Hollow mesoporous material HMS-SH containing thiol groups can be prepared *via* a common procedure.^{10,34} As shown in Fig. 13, a typical process for preparing functionalized silica hybrid materials G1 involved the following two steps: HMS-SH (1.0 g) was placed into a 20 mL sample bottle equipped with a lid. A mixture of two vinyl-containing monomers (both 0.5 mol L⁻¹, totally 5 mL) was sequentially added to the sample bottles with volume ratios of 10:0, 9:1, 7:3, 5:5, 3:7, 1:9, and 0:10 and named G1-0 to G1-6. Subsequently, an EBI treatment is performed using an AB10.0 accelerator. The sample bottle is placed on the accelerator's sample table and exposed to a 10 MeV electron beam. The actual beam current was meticulously regulated to 5.4 mA. The cumulative dose was controlled to 80 kGy. Based on previous studies,¹⁰ grafting at this dosage was deemed sufficiently effective, and all grafts were conducted at this specific dosage to comprehensively investigate the impact of the volume ratio of the grafted reagents. After finishing the irradiation, the silica material was then subjected to washing with ethanol (20 mL × 3) and ethyl acetate (20 mL × 3) to eliminate the residual monomers, followed by an overnight vacuum drying. The generality and regularity of this method were further investigated by employing several additional vinyl monomers and their combinations, as illustrated in Table 4.

4.2 Preparation of the e-HMS-PDMS coatings

The procedure for preparing the e-HMS-PDMS coatings was established according to our previous method with slight modification.³³ Polydimethylsiloxane (PDMS) and dimethyl silicone oil (DMS) were mixed in a certain mass ratio, followed by the addition of the G1–G5 hybrid materials as additives. The mass fraction of the additive was determined to be 25% based on the control experiment investigating the impact of additive content on coating hydrophilicity, as shown in Fig. S20.† The e-HMS-PDMS formulation is applied onto the substrate surface using a film coating machine, resulting in the formation of a uniform liquid film with a



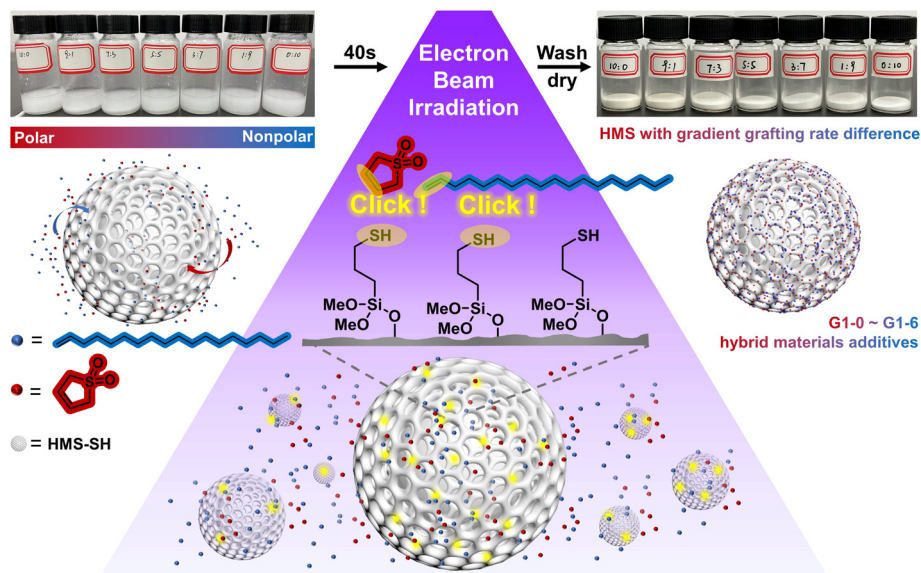


Fig. 13 The general procedure for the preparation of the EBI-grafted hybrid materials of the G1 series.

thickness of 250 microns. Subsequently, the film is exposed to irradiation and cured under nitrogen protection. The EBLab 200 accelerator can deliver an electron beam with an energy of 200 keV, while maintaining a steady current of 9.3 mA. The irradiation duration was adjusted to control the surface dose received by the coating.

4.3 Physicochemical characterization

DSC and TGA (TGA8000, PerkinElmer) tests were employed to assess the thermodynamic stability of the coating layer, while FTIR (VERTEX 70, Bruker) was utilized to examine the vibrational behavior of the chemical bonds during the radiation curing process. The G1–G5 series of HMS materials was subjected to a comprehensive investigation of the chemical and elemental compositions using FTIR (VERTEX 70, Bruker) and elemental analysis (EA, Elementar UNICUBE). Their specific surface area and pore size were meticulously characterized by BET (ASAP 2460, Micromeritics). TGA (TGA8000, PerkinElmer) was employed to assess the thermogravimetric properties within a temperature range of room temperature to 800 °C. The microstructure and surface elemental composition were characterized by utilizing FSEM (Nova NanoSEM 450, FEI) and EDS. TEM (Tecnai G2 20, FEL) was used to observe the internal structure of the HMS microspheres. The particle size distribution and zeta

potential of the HMS microspheres were characterized by nano-particle size and zeta potentiometer (BeNano 180 Zeta, Battersize). EPR (EMXmicro-6/1/P/L) was utilized to detect free radical species during the irradiation processes.

4.4 Stability test of the e-HMS-PDMS coatings

The adhesion of the coating was tested according to ASTM D3359. A blade was used to create 22 X-shaped scratches with a spacing of 1 mm on the surface of the coating. Adhesive tape was then applied to tear off and observe the percentage of coating that detached. The impact resistance was determined following ASTM D2794 by subjecting the coating to a spherical impact head falling vertically from a certain height, generating an impact force. The presence or absence of cracks and detachment of the coating before and after impact were observed to define its impact resistance. The wear resistance of the coating was verified by repeatedly rubbing it with parallel strokes using 100 g weights and 240-grit sandpaper on its surface, while also assessing its hydrophilicity through repeated measurements. The hardness characterization of the coating is determined according to ASTM D3363, primarily by examining whether pencils with different hardness can leave visible marks on the surface, thus determining its hardness level. To test solvent resistance, water, ethanol, dimethylformamide, and ethyl acetate solutions were used. A specific area of the e-HMS-PDMS coating was soaked in each solvent for 6 hours, observing any swelling or dissolution phenomena.

Table 4 Monomer selection in this study

Entry	Polar monomer	Nonpolar monomer
Group 1	3-Sulfolene	Octadec-1-ene
Group 2	<i>N,N'</i> -Methylenebisacrylamide	Octadec-1-ene
Group 3	Vinylacetic acid	Octadec-1-ene
Group 4	Acrylonitrile	Styrene
Group 5	Acrylonitrile	Octadec-1-ene

Author contributions

Haozhe Li: conceptualization, investigation, data curation, formal analysis, visualization, writing – original draft and writing – review & editing. Keyan Sheng: methodology, visualization and writing – review & editing. Zhiyan Chen: data curation and validation. Shuai Hao: validation. Zijian



Zhou: writing – review & editing. Zhenyi Zhang: validation. Xinwen Liu: formal analysis. Mianzhi Xiong: visualization. Yanlong Gu: funding acquisition, conceptualization, resources, project administration and supervision. Jiang Huang: funding acquisition, conceptualization, resources, project administration and supervision.

Conflicts of interest

There are no conflicts to declare.

Acknowledgements

This work was supported by the Program for HUST Academic Frontier Youth Team (2019QYTD06) and Natural Science Foundation of Wuhan. Caiyun Ding is also thanked for her careful guidance in the drawing and typesetting process.

References

- J. Drelich, E. Chibowski, D. D. Meng and K. Terpilowski, Hydrophilic and superhydrophilic surfaces and materials, *Soft Matter*, 2011, **7**, 9804–9828.
- X. Chang, M. Li, S. Tang, L. Shi, X. Chen, S. Niu, X. Zhu, D. Wang and S. Sun, Superhydrophobic micro-nano structured PTFE/WO₃ coating on low-temperature steel with outstanding anti-pollution, anti-icing, and anti-fouling performance, *Surf. Coat. Technol.*, 2022, **434**, 128214.
- C. Qiu, W. Xiong, H. Zhang, R. Zhang, I. P. Parkin, S. Wang, L. Li, J. Chen, Z. Chen, A. R. Tapa, A. Trokourey, W. Zhou, X. Zhao and Y. Xie, Superhydrophobicity transfer effect in superwetting coatings for strengthening anti-pollution flashover performance, *Prog. Org. Coat.*, 2024, **186**, 107955.
- M. Lotfi, M. Nejib and M. Naceur, Cell adhesion to biomaterials: Concept of biocompatibility, *Adv. in bio. sci. and biomed. appl.*, 2013, vol. 8, pp. 207–240.
- C. Yang, M. Long, C. Ding, R. Zhang, S. Zhang, J. Yuan, K. Zhi, Z. Yin, Y. Zheng, Y. Liu, H. Wu and Z. Jiang, Antifouling graphene oxide membranes for oil-water separation via hydrophobic chain engineering, *Nat. Commun.*, 2022, **13**, 7334.
- X. Cheng, T. Li, L. Yan, Y. Jiao, Y. Zhang, K. Wang, Z. Cheng, J. Ma and L. Shao, Biodegradable electrospinning superhydrophilic nanofiber membranes for ultrafast oil-water separation, *Sci. Adv.*, 2023, **9**, eadh8195.
- C. S. Sujith Kumar, S. Suresh, A. S. Praveen, M. C. Santhosh Kumar and V. Gopi, Effect of surfactant addition on hydrophilicity of ZnO–Al₂O₃ composite and enhancement of flow boiling heat transfer, *Exp. Therm. Fluid Sci.*, 2016, **70**, 325–334.
- X. Zhang, J. Li, H. Ao, D. Liu, L. Shi, C. Wang, Y. Zhu and Y. Qian, Appropriately hydrophilic/hydrophobic cathode enables high-performance aqueous zinc-ion batteries, *Energy Storage Mater.*, 2020, **30**, 337–345.
- S. Li, Y. Liu, X. Zhao, Q. Shen, W. Zhao, Q. Tan, N. Zhang, P. Li, L. Jiao and X. Qu, Sandwich-like heterostructures of MoS₂/graphene with enlarged interlayer spacing and enhanced hydrophilicity as high-performance cathodes for aqueous zinc-ion batteries, *Adv. Mater.*, 2021, **33**, 2007480.
- Z. Chen, H. Li, K. Sheng, X. Dong, J. Yuan, S. Hao, M. Li, R. Bai, Y. Queneau, A. Sidorenko, J. Huang and Y. Gu, Dipolar modification in heterogeneous catalysts under electron beam irradiation for the conversion of biomass-derived platform molecules, *ACS Catal.*, 2022, **12**, 15618–15625.
- V. Muhr, S. Wilhelm, T. Hirsch and O. S. Wolfbeis, Upconversion nanoparticles: From hydrophobic to hydrophilic surfaces, *Acc. Chem. Res.*, 2014, **47**, 3481–3493.
- S. L. Gras, T. Mahmud, G. Rosengarten, A. Mitchell and K. Kalantar-zadeh, Intelligent control of surface hydrophobicity, *ChemPhysChem*, 2007, **8**, 2036–2050.
- M. Vallet, B. Berge and L. Vovelle, Electrowetting of water and aqueous solutions on poly(ethylene terephthalate) insulating films, *Polymer*, 1996, **37**, 2465–2470.
- M. Vallet, M. Vallade and B. Berge, Limiting phenomena for the spreading of water on polymer films by electrowetting, *Eur. Phys. J. B*, 1999, **11**, 583–591.
- J. Sondag-Huethorst and L. Fokkink, Potential-dependent wetting of electroactive ferrocene-terminated alkanethiolate monolayers on gold, *Langmuir*, 1994, **10**, 4380–4387.
- K. Ichimura, S.-K. Oh and M. Nakagawa, Light-driven motion of liquids on a photoresponsive surface, *Science*, 2000, **288**, 1624–1626.
- X. Feng, L. Feng, M. Jin, J. Zhai, L. Jiang and D. Zhu, Reversible super-hydrophobicity to super-hydrophilicity transition of aligned ZnO nanorod films, *J. Am. Chem. Soc.*, 2004, **126**, 62–63.
- T. Sun, G. Wang, L. Feng, B. Liu, Y. Ma, L. Jiang and D. Zhu, Reversible switching between superhydrophilicity and superhydrophobicity, *Angew. Chem., Int. Ed.*, 2004, **43**, 357–360.
- J. Zhang, X. Lu, W. Huang and Y. Han, Reversible superhydrophobicity to superhydrophilicity transition by extending and unloading an elastic polyamide film, *Macromol. Rapid Commun.*, 2005, **26**, 477–480.
- J. Chen, H. Wang, X. Liu, X. Han and H. Liu, Multiple methods to control the hydrophilic–hydrophobic balance of P(DMA-co-DMAEMA-co-QDMAEMA) coatings, *Soft Matter*, 2022, **18**, 4913–4922.
- W. Xie, Y. Guo, J. Li, H. Liu and J. Hu, Hydrophobicity regulation by a facial bromine substitution in MIL-47(V) for highly selective adsorptive desulfurization, *AIChE J.*, 2023, **69**, e17933.
- Q.-X. Mao, W. J. Wang, X. Hai, Y. Shu, X.-W. Chen and J.-H. Wang, The regulation of hydrophilicity and hydrophobicity of carbon dots via a one-pot approach, *J. Mater. Chem. B*, 2015, **3**, 6013–6018.
- N. Sharifi, M. Pugh, C. Moreau and A. Dolatabadi, Developing hydrophobic and superhydrophobic TiO₂ coatings by plasma spraying, *Surf. Coat. Technol.*, 2016, **289**, 29–36.
- R. D. Mshelia, N. I. Dibal and S. M. Chiroma, Food irradiation: An effective but under-utilized technique for food preservations, *J. Food Sci. Technol.*, 2023, **60**, 2517–2525.
- C. L. Duarte, M. H. O. Sampa, P. R. Rela, H. Oikawa, E. H. Cherbakian, H. C. Sena, H. Abe and V. Sciani, Application of electron beam irradiation combined to conventional



- treatment to treat industrial effluents, *Radiat. Phys. Chem.*, 2000, **57**, 513–518.
- 26 J. Pusch and A. M. van Herk, Pulsed electron beam initiation in emulsion polymerization, *Macromolecules*, 2005, **38**, 8694–8700.
- 27 W. A. Parejo Calvo, C. L. Duarte, L. D. B. Machado, J. E. Manzoli, A. B. C. Geraldo, Y. Kodama, L. G. A. Silva, E. S. Pino, E. S. R. Somessari, C. G. Silveira and P. R. Rela, Electron beam accelerators—trends in radiation processing technology for industrial and environmental applications in Latin America and the Caribbean, *Radiat. Phys. Chem.*, 2012, **81**, 1276–1281.
- 28 A. Schulze, M. F. Maitz, R. Zimmermann, B. Marquardt, M. Fischer, C. Werner, M. Went and I. Thomas, Permanent surface modification by electron-beam-induced grafting of hydrophilic polymers to PVDF membranes, *RSC Adv.*, 2013, **3**, 22518–22526.
- 29 M. S. Ibrahim, K. M. E. Salmawi and S. M. Ibrahim, Electron-beam modification of textile fabrics for hydrophilic finishing, *Appl. Surf. Sci.*, 2005, **241**, 309–320.
- 30 L. Wang, K. Wang, N. Erkan, Y. Yuan, J. Chen, B. Nie, F. Li and K. Okamoto, Metal material surface wettability increase induced by electron beam irradiation, *Appl. Surf. Sci.*, 2020, **511**, 145555.
- 31 H. Zhao, C. Zhang, B. Yang, X. Zhang, X. Dong, D. Wang and G. Liu, Achieving high elasticity of trans-1, 4-polyisoprene with a combination of radiation crosslinking and thiol-ene grafting, *Polym. Chem.*, 2023, **14**, 81–91.
- 32 R. Zandi Shafagh, A. Vastesson, W. Guo, W. van der Wijngaart and T. Haraldsson, E-beam nanostructuring and direct click biofunctionalization of thiol-ene resist, *ACS Nano*, 2018, **12**, 9940–9946.
- 33 K. Sheng, X. Dong, H. Li, Z. Zhou, W. Zhou, T. Zeng, X. Liu, Z. Chen, M. Xiong, Z. Zhang, K. Ning, Y. Gu and J. Huang, Electron beam in-situ ultrafast curing of loadable primer-free polydimethylsiloxane coatings for composite insulators, *Appl. Surf. Sci.*, 2023, **621**, 156830.
- 34 G. Qi, Y. Wang, L. Estevez, A. K. Switzer, X. Duan, X. Yang and E. P. Giannelis, Facile and scalable synthesis of monodispersed spherical capsules with a mesoporous shell, *Chem. Mater.*, 2010, **22**, 2693–2695.
- 35 J. Zhang, H. Duan, J. Zou, J. Cao, C. Wan, C. Zhang and H. Ma, A DOPO derivative constructed by sulfaguanidine and thiophene toward enhancing fire safety, smoke suppression, and mechanical properties of epoxy resin, *Macromol. Mater. Eng.*, 2021, **306**, 2100569.
- 36 S. Dutta, M. Perring, S. Barrett, M. Mitchell, P. J. A. Kenis and N. B. Bowden, Cross metathesis on olefin-terminated monolayers on Si(111) using the Grubbs' catalyst, *Langmuir*, 2006, **22**, 2146–2155.
- 37 Q. Sun, B. Aguila, J. Perman, L. D. Earl, C. W. Abney, Y. Cheng, H. Wei, N. Nguyen, L. Wojtas and S. Ma, Postsynthetically modified covalent organic frameworks for efficient and effective mercury removal, *J. Am. Chem. Soc.*, 2017, **139**, 2786–2793.
- 38 D. Zhu, H. Zhang, Q. Tao, Z. Xu and S. Zheng, Surface functionalized mesoporous silicas as adsorbents for aromatic contaminants in aqueous solution, *Environ. Toxicol. Chem.*, 2009, **28**, 1400–1408.
- 39 P. T. Tanev and T. J. Pinnavaia, A neutral templating route to mesoporous molecular sieves, *Science*, 1995, **267**, 865–867.
- 40 M. B. Yue, L. B. Sun, Y. Cao, Y. Wang, Z. J. Wang and J. H. Zhu, Efficient CO₂ capturer derived from As-synthesized MCM-41 modified with amine, *Chem. – Eur. J.*, 2008, **14**, 3442–3451.
- 41 T. Liu, G. Li, N. Zhang and Y. Chen, An inorganic–organic hybrid optical sensor for heavy metal ion detection based on immobilizing 4-(2-pyridylazo)-resorcinol on functionalized HMS, *J. Hazard. Mater.*, 2012, **201–202**, 155–161.
- 42 T. A. Zepeda, J. L. G. Fierro, B. Pawelec, R. Nava, T. Klimova, G. A. Fuentes and T. Halachev, Synthesis and characterization of Ti-HMS and CoMo/Ti-HMS oxide materials with varying Ti content, *Chem. Mater.*, 2005, **17**, 4062–4073.
- 43 E. E. Beasley and R. S. Anderson, Electron spin resonance of ultraviolet-irradiated compounds. II. Peroxide-initiated radicals in straight chain alkenes, *J. Chem. Phys.*, 1964, **40**, 2565–2572.
- 44 D. Griller, J. W. Cooper and K. U. Ingold, Kinetic applications of electron paramagnetic resonance spectroscopy. XVIII. Persistent vinyl, alkyl, and allyl radicals, *J. Am. Chem. Soc.*, 1975, **97**, 4269–4275.
- 45 G. R. Buettner, Spin trapping: ESR parameters of spin adducts 1474 1528V, *Free Radical Biol. Med.*, 1987, **3**, 259–303.
- 46 M. Saravanan, S. Sudalai, A. B. Dharaneesh, V. Prahaaladhan, G. Srinivasan and A. Arumugam, An extensive review on mesoporous silica from inexpensive resources: Properties, synthesis, and application toward modern technologies, *J. Sol-Gel Sci. Technol.*, 2023, **105**, 1–29.
- 47 H. Yang, Q. T. Nguyen, Y. Ding, Y. Long and Z. Ping, Investigation of poly(dimethyl siloxane) (PDMS)–solvent interactions by DSC, *J. Membr. Sci.*, 2000, **164**, 37–43.
- 48 Z. Karami, O. M. Jazani, A. H. Navarchian and M. R. Saeb, State of cure in silicone/clay nanocomposite coatings: The puzzle and the solution, *Prog. Org. Coat.*, 2018, **125**, 222–233.
- 49 Z. Karami, O. M. Jazani, A. H. Navarchian and M. R. Saeb, Cure kinetics of silicone/halloysite nanotube composites, *J. Vinyl Addit. Technol.*, 2020, **26**, 548–565.
- 50 H. Menhofer and H. Heusinger, Radical formation in polydimethylsiloxanes and polydimethyldiphenylsiloxanes studied by the ESR spintrap technique, *Radiat. Phys. Chem.*, 1987, **29**, 243–251.
- 51 L. Schilinsky, G. Jeschke, R. Tschaggelar, R. Wilken and D. Klose, Formation and decay of radicals during Vacuum-UV irradiation of poly(dimethylsiloxane), *Polym. Degrad. Stab.*, 2017, **144**, 497–507.
- 52 S. I. Ohnishi, T. Tanei and I. Nitta, ESR study of free radicals produced by irradiation in benzene and its derivatives, *J. Chem. Phys.*, 2004, **37**, 2402–2407.
- 53 L. E. M. Gevers, I. F. J. Vankelecom and P. A. Jacobs, Solvent-resistant nanofiltration with filled polydimethylsiloxane (PDMS) membranes, *J. Membr. Sci.*, 2006, **278**, 199–204.

